Supporting information

Improved Oxygen Reduction Reaction Performance of Co Confined in Ordered N-doped Porous Carbon Derived from ZIF-67@PILs

Xiang Zhou, Yi-jing Gao, Sheng-wei Deng, Shan Cheng, Shao-hua Zhang, Hui Hu, Gui-lin Zhuang,* Xing Zhong, Jian-guo Wang*

[a]Institute of Industrial Catalysis, College of Chemical Engineering, Zhejiang University of Technology, Hangzhou, P.R.China, 310032

Email: glzhuang@zjut.edu.cn (G.L.Zhuang), jgw@zjut.edu.cn (J.g.Wang)

1. STRUCTURE CHARACTERIZATION

The morphologies of samples and elemental population were observed High performance transmission electron microscopy (HR-TEM, Tecnai G2 F30) and scanning electron microscopy (SEM, Hitachi S4700). Powder X-ray diffraction (PXRD) patterns were recorded in a Panalytical X-Pert pro diffractometer with Cu-Kα radiation. Thermal stability was identified by the thermal gravimetric analyzer (SDT Q600, TA Instruments Co.) with heating rate of 10°C ·min^{-1} from room temperature to 800^{o}C in an Ar atmosphere. X-ray photoelectron measurements were conducted on a Kratos AXIS Ultra DLD instruments using 300W Al Ka radiation and C 1s peak at 284.5 eV as internal standard. The surfaces area of the samples were obtained by the measuring nitrogen adsorption isothermal in an Surface properties analyzer instrument (3Flex, Micromeritics). Raman spectra were recorded with a Renishaw 2000 model confocal microscopy Raman spectrometer.

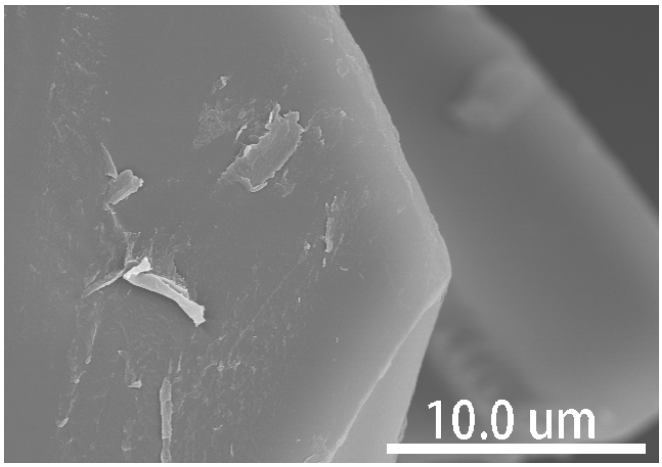

Figure S1 SEM image of the as-synthesized PILs.

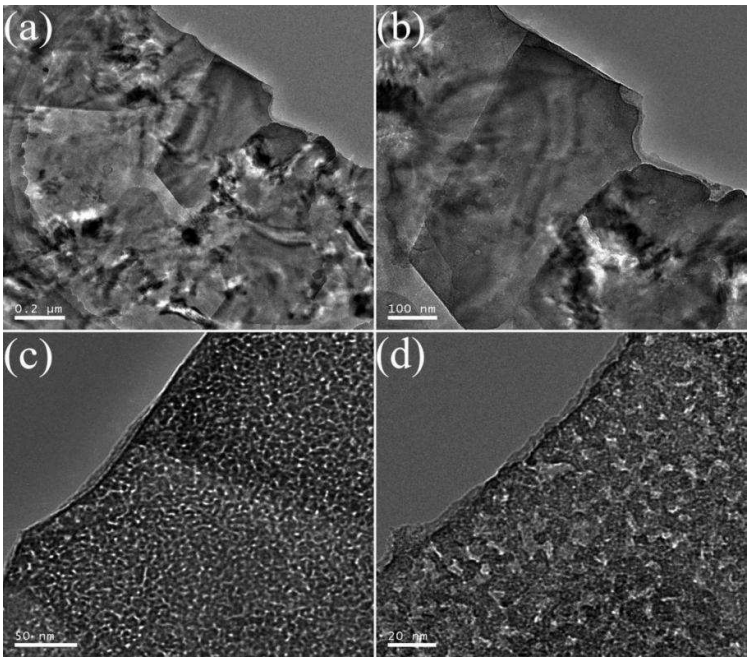

Figure S2 (a) – (d) TEM images of the as-prepared NC sample.

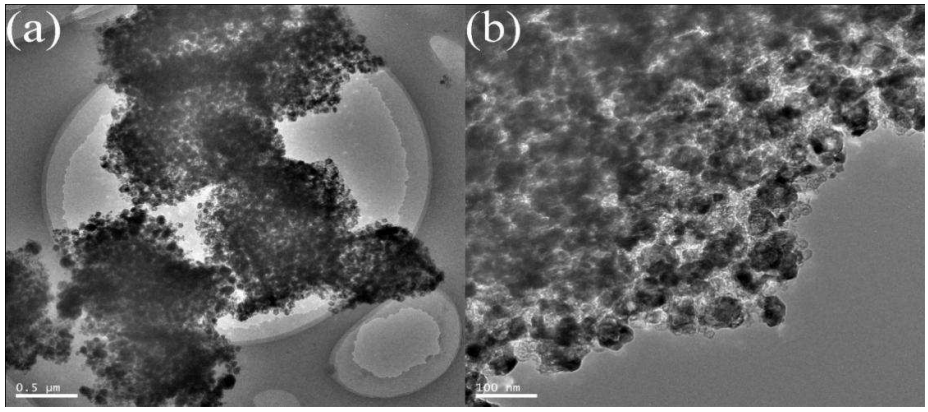

Figure S3 (a) and (b) TEM images of the Co@O-NPC (without acid treatment) sample.

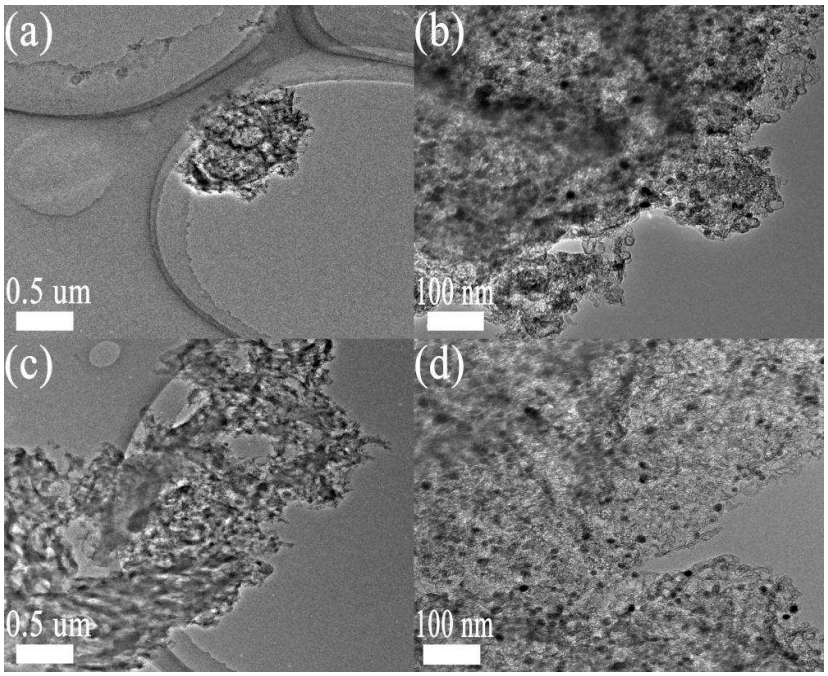

Figure S4 TEM images of the Co@O-NPC-600 (a – b) and Co@O-NPC-800 (c – d), respectively.

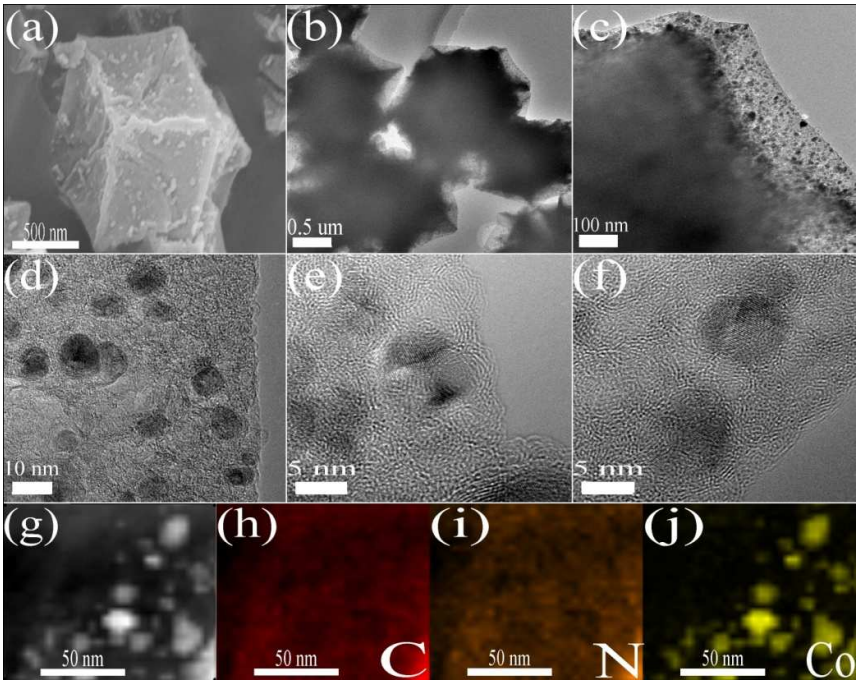

Figure S5 (a) SEM image of Co@DO-NPC. (b) – (f) TEM images (Figure(b) and (c)) and HRTEM images (Figure(d) – (f))of Co@DO-NPC., and (g) STEM image of the sample Co@DO-NPC.. (h) – (j) element mapping images of carbon, nitrogen and cobalt, respectively.

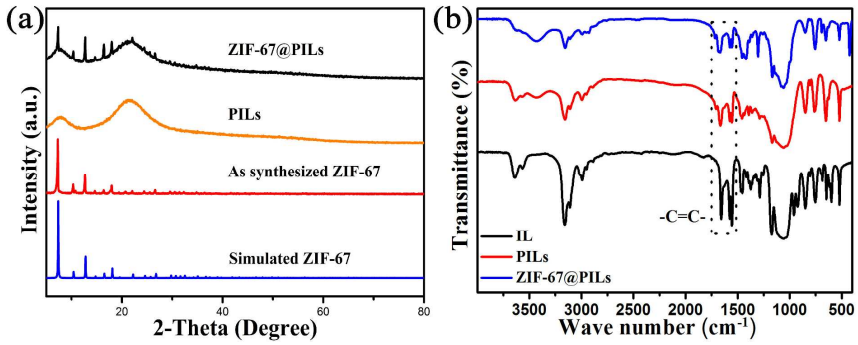

Figure S6 (a) XRD patterns of Simulated ZIF-67, the as-synthesized ZIF-67, poly ionic liquids (PILs) and the ZIF-67@PILs composites respectively. (b) FT-IR spectra of ionic liquids (IL), poly ionic liquids (PILs) and the ZIF-67@PILs composites.

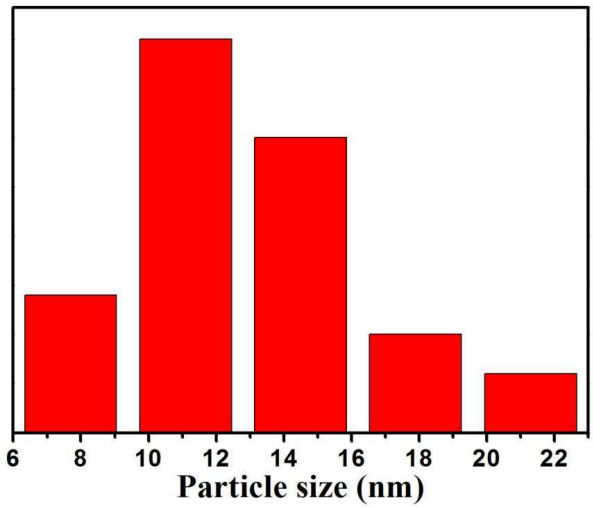

Figure S7 Co particles-size distribution of the Co@O-NPC sample calculated from HR-TEM results

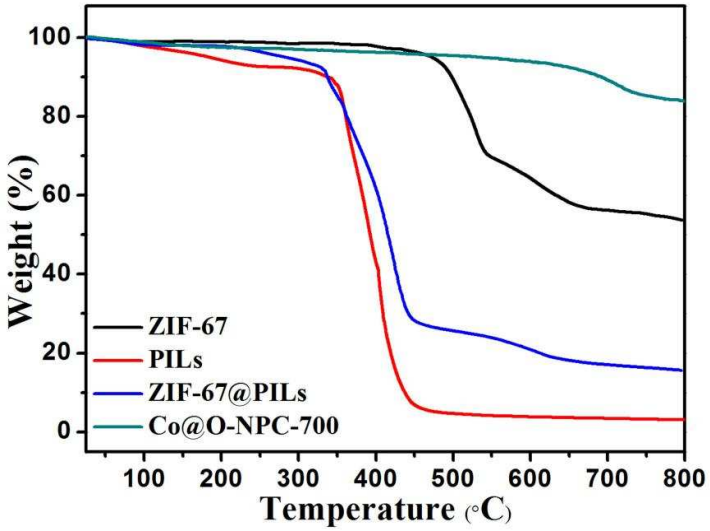

Figure S8 TGA curve of the as-synthesized ZIF-67 precursor, PILs, ZIF-67@PILs composites and the Co@O-NPC-700 sample, respectively.

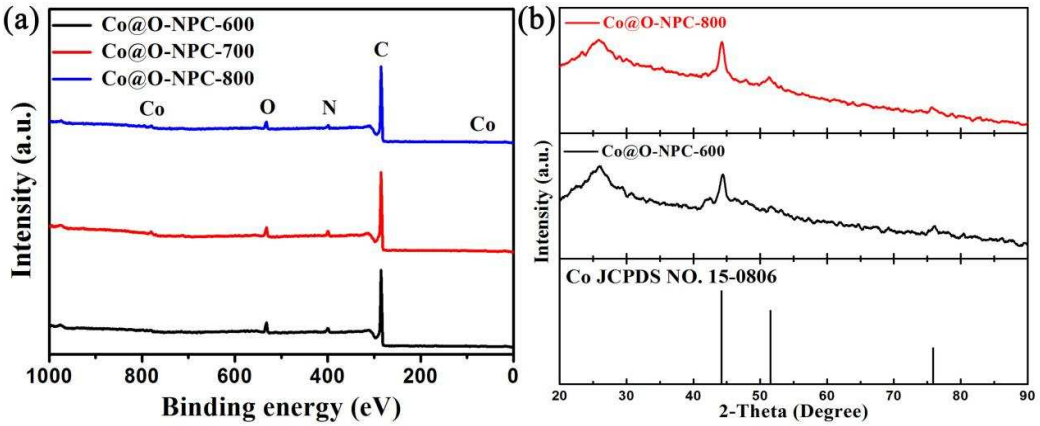

Figure S9 (a) XPS analysis results of the as-prepared Co@O-NPC-600, Co@O-NPC-700 and Co@O-NPC-800 samples. (b) XRD patterns of Co@O-NPC-600 and Co@O-NPC-800 samples.

Table S1 Elemental composition (atomic percentage) obtained from XPS analysis.

	C	N	O	Co
Co@O-NPC-600	**87.37**	**5.49**	**6.56**	**0.58**
Co@O-NPC-700	**87.61**	**6.27**	**5.45**	**0.67**
Co@O-NPC-800	**90.36**	**4.41**	**4.41**	**0.62**
Co@DO-NPC	**80.88**	**9.50**	**4.87**	**4.76**

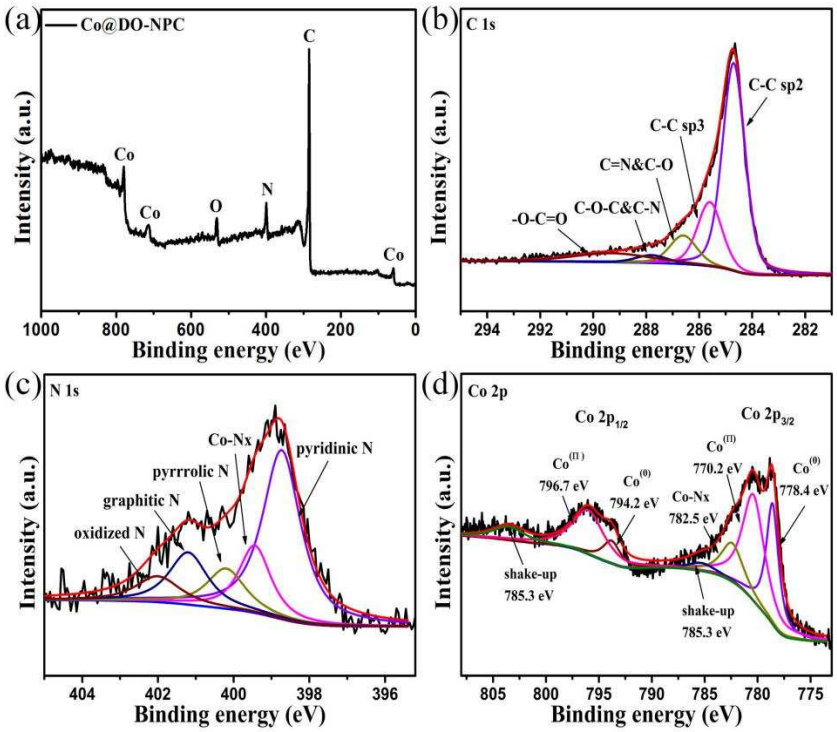

Figure S10 (a) XPS analysis results of the as-prepared Co@DO-NPC-700. (b) - (d) High-resolution XPS spectra of C 1s (b), N 1s (c), Co 2p (d), respectively.

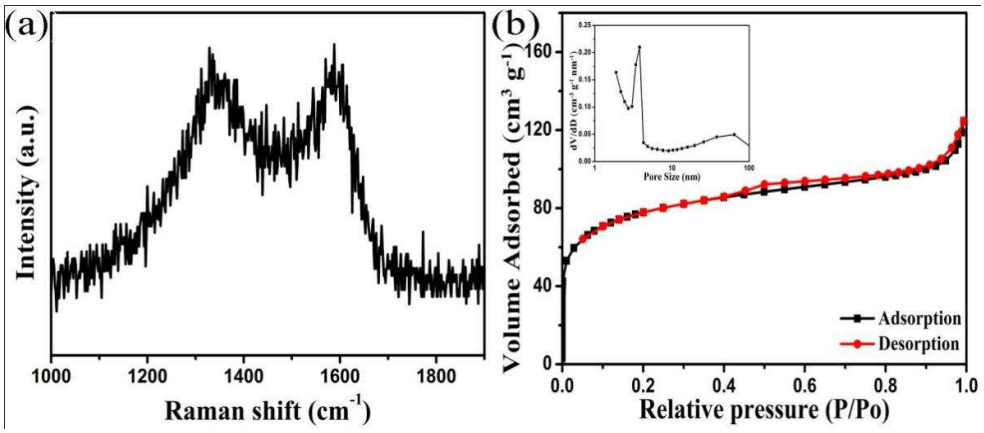

Figure S11 (a) Raman spectra of the as-prepared Co@DO-NPC sample. (b) N2 adsorption – desorption isotherms of the Co@DO-NPC sample. The inset in (b) shows the pore size distribution curve.

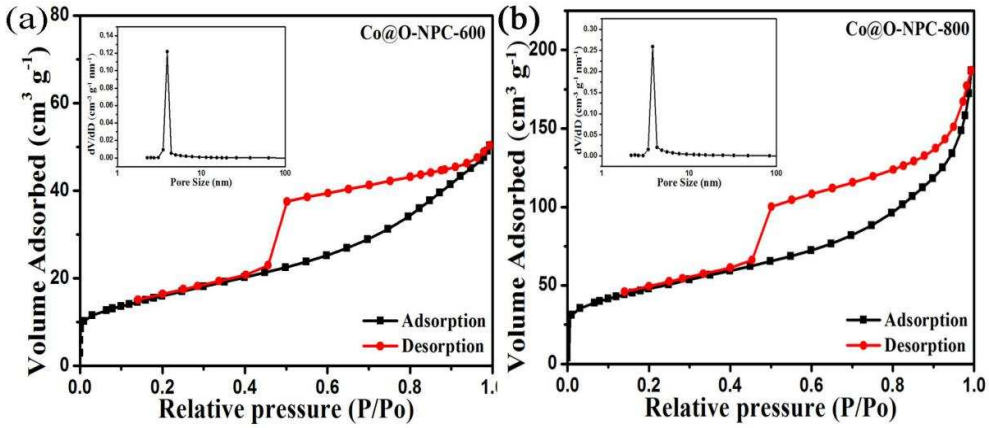

Figure S12 N_2 adsorption-desorption isotherms of the sample Co@O-NPC-600 (a) and Co@O-NPC-800 (b), respectively. The inset in (a) and (b) were the pore size distribution curve.

2. ELECTRICHEMICAL PROPERTY MEASUREMENT

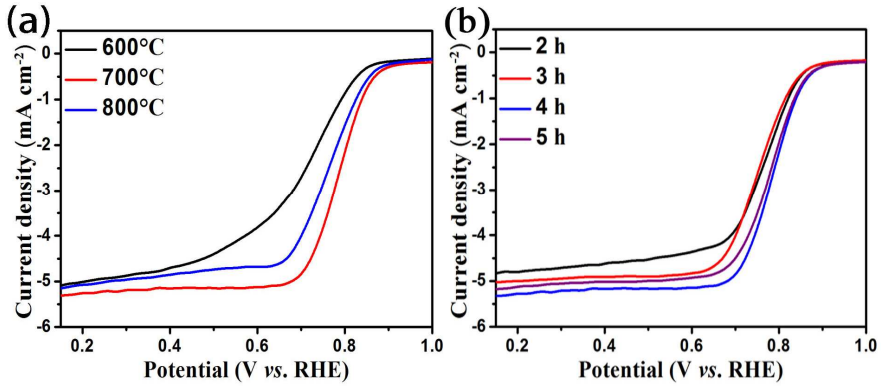

Figure S13 LSV curves of the as-prepared Co@O-NPC obtained at different temperatures for 4 hours (a), and different calcination times under 700°C (b).

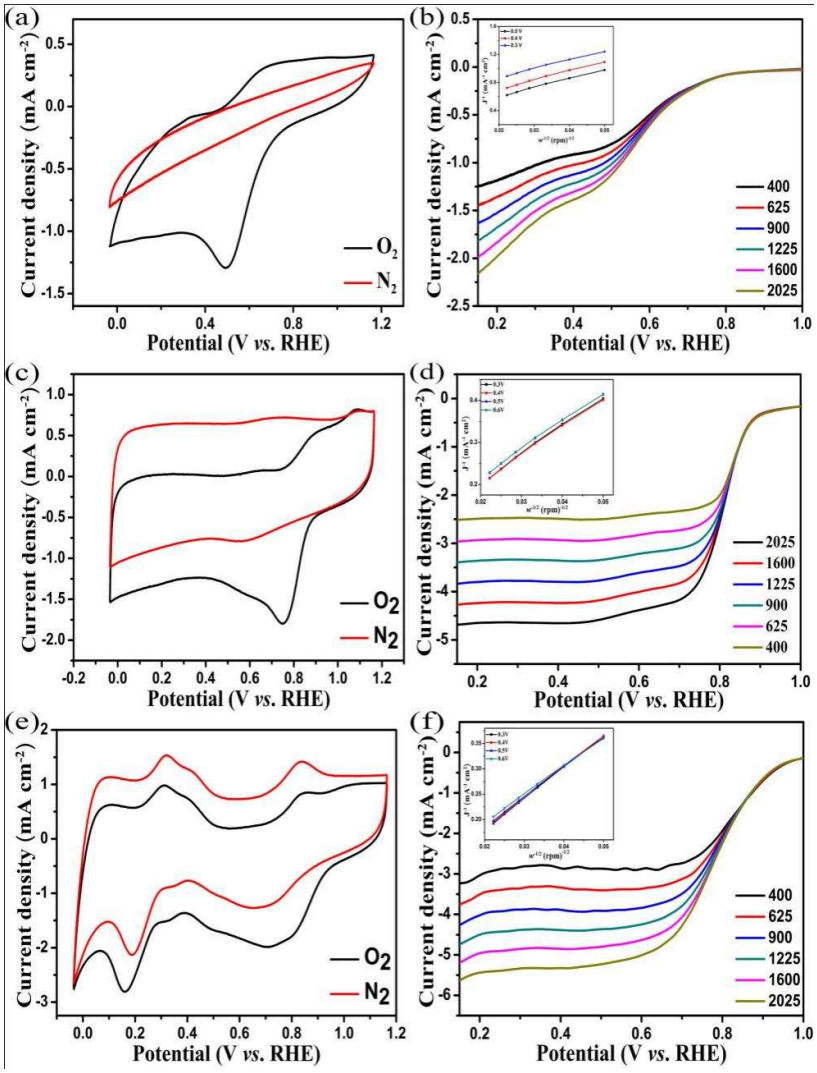

Figure S14 CV profiles of the NC (a) Co@DO-NPC-700 (c) and Pt/C (e) in O_2- (black curves) and N_2- (red curves) saturated 0.1M KOH solution with a scan rate of 100 mV s^{-1}. LSV results different rotation rates of the NC (b) Co@DO-NPC-700 (d) and Pt/C (f) samples. The inset pictures show the corresponding K-L plots at different potentials.

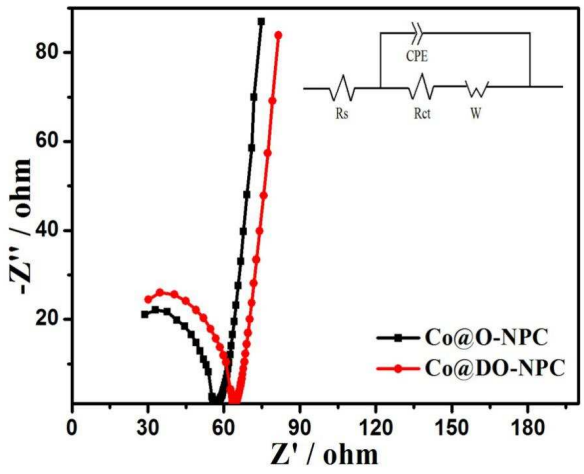

Figure S15 Nyquist ploys of Co@O-NPC-700 and Co@DO-NPC-700 at a bias of open potential (0.9 V *vs.* RHE) in O_2 - saturated 0.1 M KOH solution.

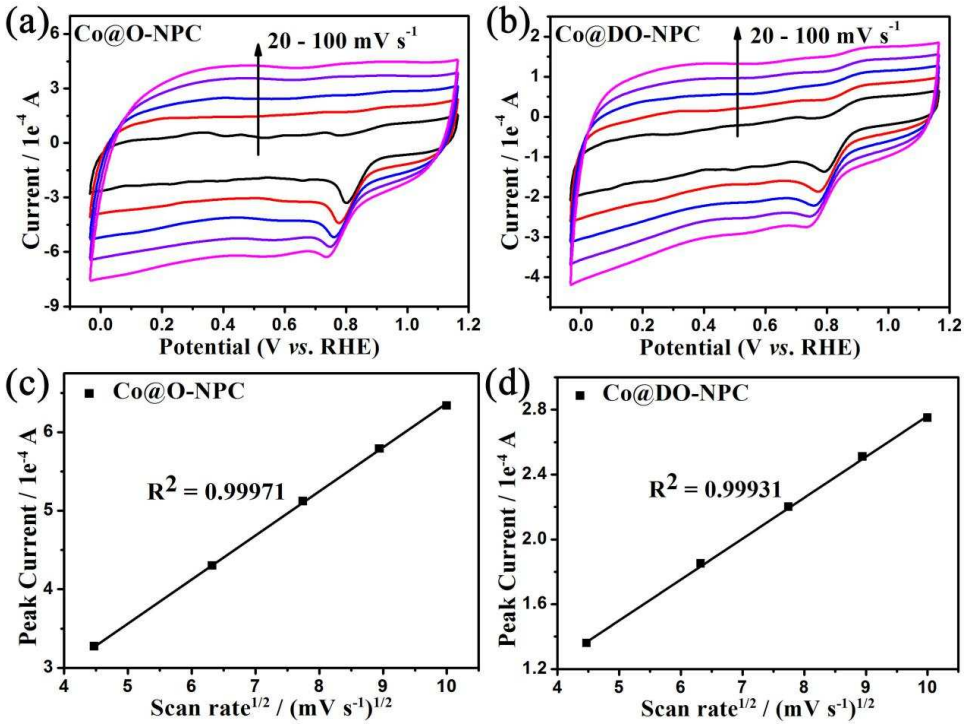

Figure S16 CV profiles at different scan rate of Co@O-NPC-700 (a) and Co@DO-NPC-700 (b) in O2-saturated 0.1 M KOH electrolyte. The linear relationships between Peak Current and the square root of scanning rate of Co@O-NPC-700 (c) and Co@DO-NPC-700 (d).

3. THEORETICAL RESULTS

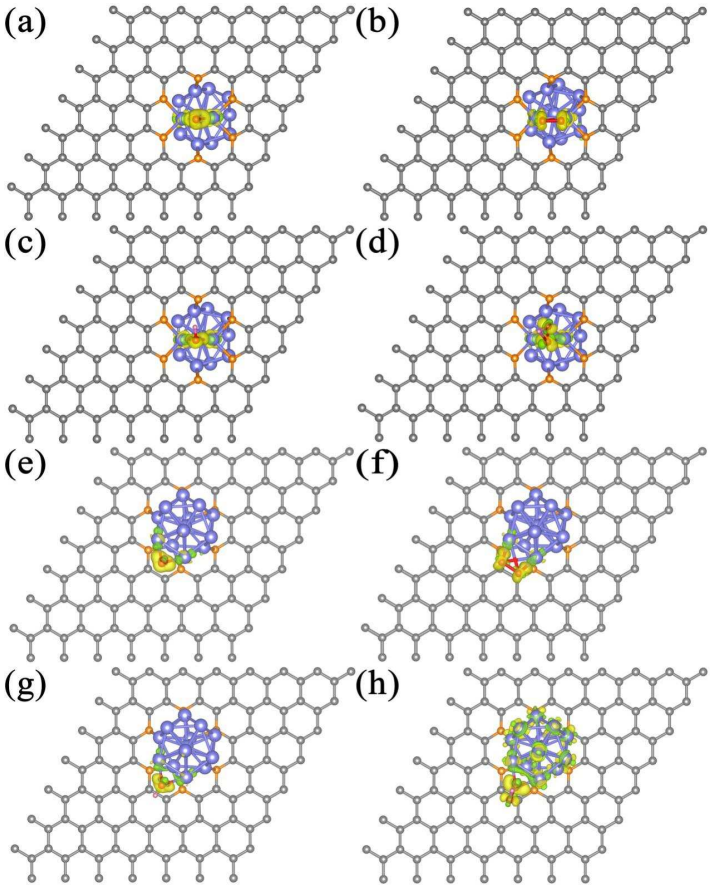

Figure S17 Charge difference figure of adsorption configuration of reaction species on bottom (a – d) and top (e - h) site of Co@NPC.

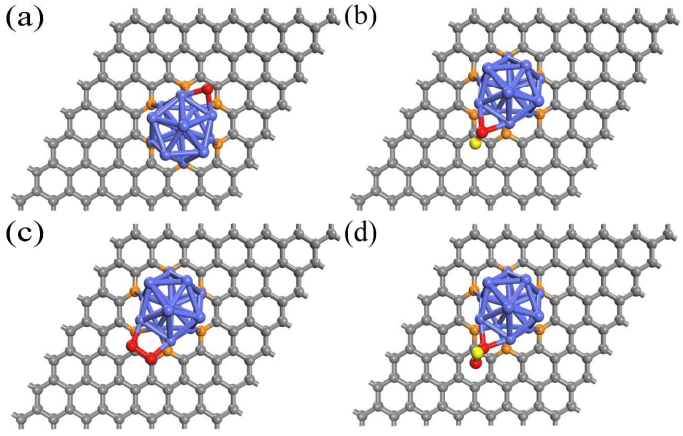

Figure S18 adsorption structure of O_2/ Co@NPC (a), O/ Co@NPC (b), OH/ Co@NPC (c) and OOH/Co@NPC (d) on the top site.

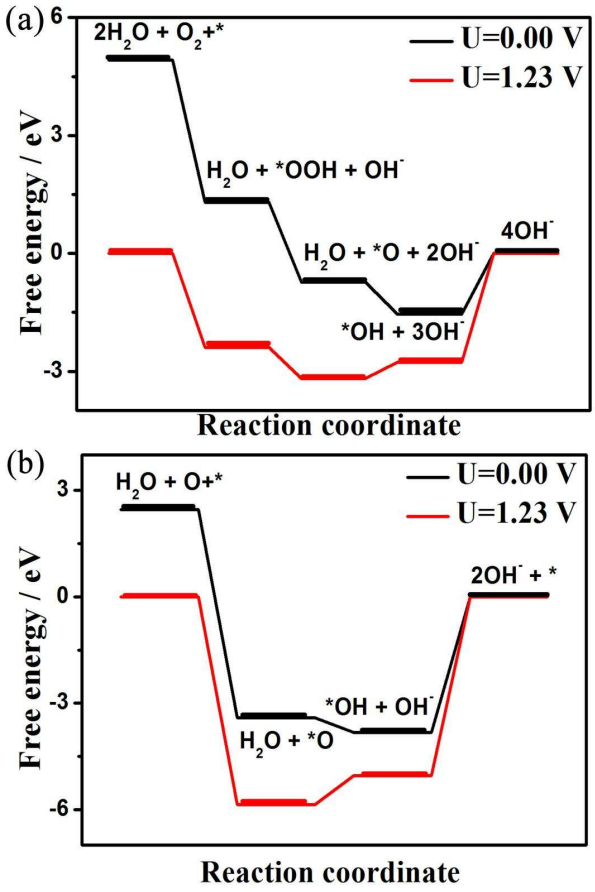

Figure S19 Diagram of free energy at U = 0 and 1.23 V for the top site of Co@O-NPC under two different mechanisms: associative (a) and dissociative mechanisms (b).

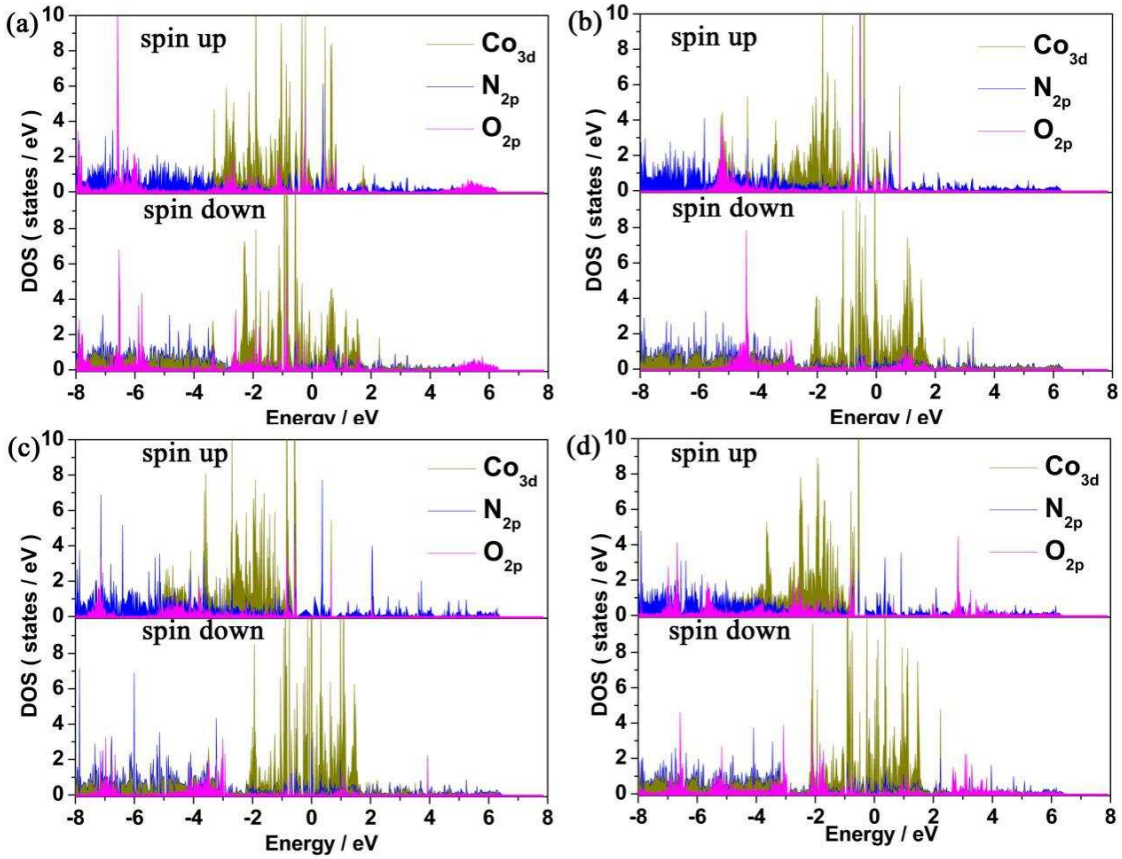

Figure S20 Partial Density of state of Co, O and N in O2/ Co@O-NPC (a), O2/ Co@O-NPC (b), OH/ Co@O-NPC (c) and OOH/ Co@O-NPC (d).

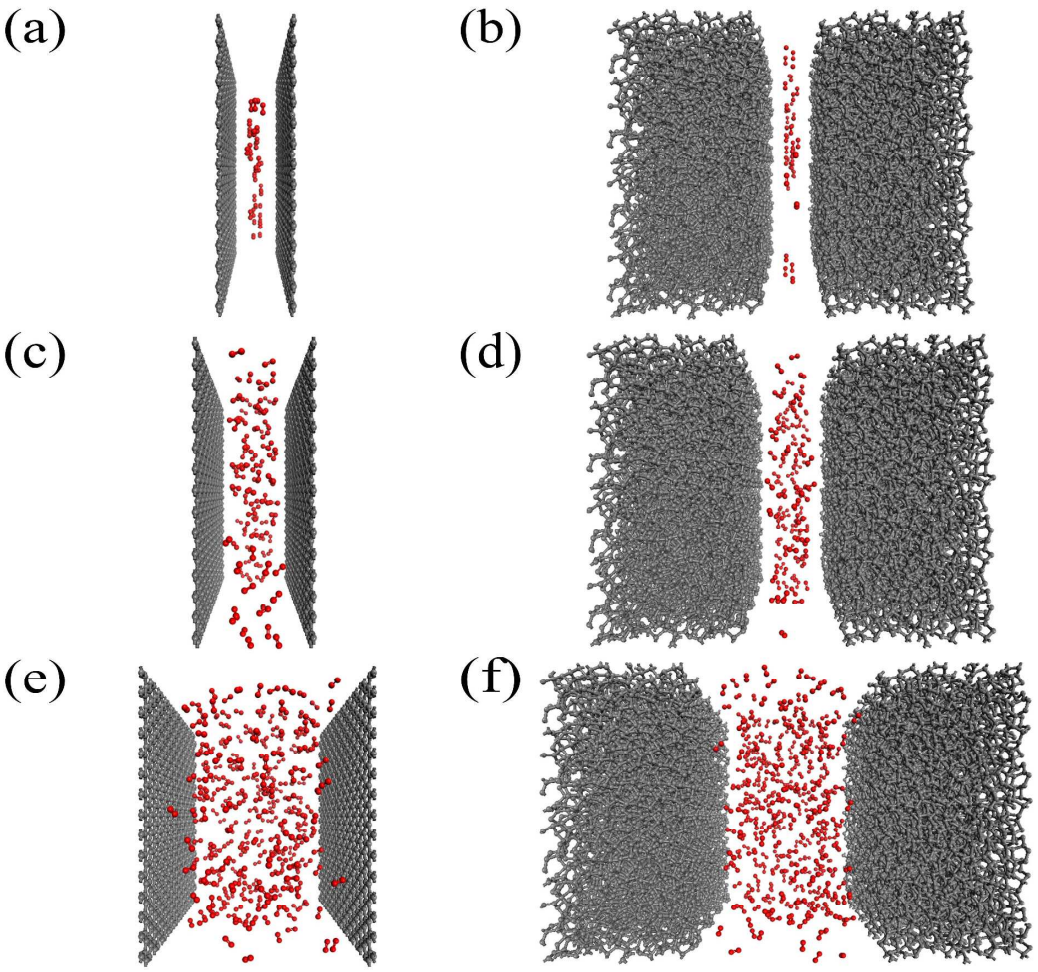

Figure S21 Illustrative snapshots of the system at the end of the 1.1 ns MD simulation for O_2 confined with different confined widths in graphene (a, c and e) and amorphous carbon (b, d and f) with different confined widths.

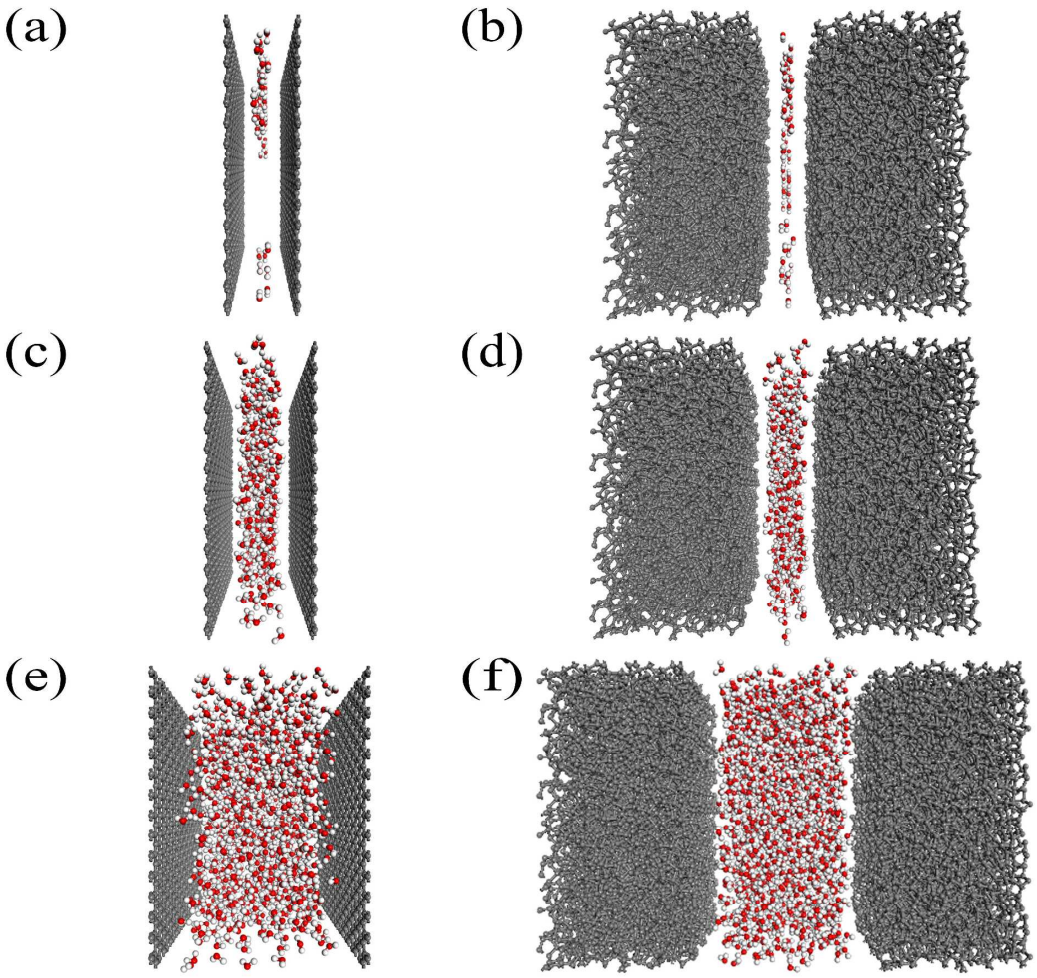

Figure S22 Illustrative snapshots of the system at the end of the 1.1 ns MD simulation for H_2O confined with different confined widths in graphene (a, c and e) and amorphous carbon (b, d and f) with different confined widths.